Head and neck tumors angiogenesis imaging with ^{68}Ga-NODAGA-RGD in comparison to ^{18}F-FDG PET/CT: A pilot study.

Steve Durante
Centre Hospitalier Universitaire Vaudois https://orcid.org/0000-0002-4067-315X
Vincent Dunet (vincent.dunet@chuv.ch)
Centre Hospitalier Universitaire Vaudois https://orcid.org/0000-0002-9897-4561
François Gorostidi
Centre Hospitalier Universitaire Vaudois
Periklis Mitsakis
Centre Hospitalier Universitaire Vaudois
Niklaus Schaefer
Centre Hospitalier Universitaire Vaudois
Judith Delage
Centre Hospitalier Universitaire Vaudois
John O. Prior
Centre Hospitalier Universitaire Vaudois

Original research

Keywords: Head and neck cancer, PET, 18F-FDG, 68Ga-NODAGA-RGD, angiogenesis

Posted Date: May 5th, 2020

DOI: https://doi.org/10.21203/rs.3.rs-19910/v2

Version of Record: A version of this preprint was published at EJNMMI Research on May 7th, 2020. See the published version at https://doi.org/10.1186/s13550-020-00638-w.

Abstract

Background : Angiogenesis plays an important role in head and neck squamous cell carcinomas (HNSCC) progression. This pilot study was designed to compare the distribution of 68 Ga-NODAGA-RGD PET/CT for imaging α v β 3 integrins involved in tumor angiogenesis to 18 F-FDG PET/CT in patients with HNSCC.

Material and methods : Ten patients (aged: 58.4 ± 8.3 years [range: 44–73 years], 6 males, 4 females) with a total of 11 HNSCC were prospectively enrolled. Activity mapping and standard uptake values (SUV) from both 68 Ga -NODAGA-RGD and 18 F-FDG PET/CT scans were recorded for primary tumor and compared with the Wilcoxon signed-rank test. The relation between the SUV of both tracers was assessed using the Spearman correlation.

Results : All HNSCC tumors were visible with both tracers. Quantitative analysis showed higher 18 F-FDG SUV max in comparison to 68 Ga-NODAGA-RGD (14.0 ± 6.1 versus 3.9 ± 1.1 g/mL, p=0.0017) and SUV mean (8.2 ± 3.1 versus 2.0 ± 0.8 g/mL, p=0.0017). Both 18 F-FDG and 68 Ga-NODAGA-RGD uptake were neither correlated with grade, HPV nor p16 protein expression (p≥0.17).

Conclusion : All HNSCC tumors were detected with both tracers with higher uptake with 18 F-FDG, however. 68 Ga-NODAGA-RGD has a different spatial distribution than 18 F-FDG bringing different tumor information.

Background

Cancer is the second cause of mortality and morbidity in industrial countries and is expected to become even more predominant in the future. Head and neck tumors are frequent and represent in Switzerland an incidence of roughly 1,000 new cases annually. Around 70% of them are diagnosed in advanced stages with a five-year survival rate of 50% [1, 2]. Excessive alcohol consumption and smoking are commonly encountered in most head and neck squamous cell carcinoma (HNSCC) patients aged 55 years and older. In the last ten years, the incidence of HNSCC in Western countries has increased due to rising incidence of human papillomavirus (HPV)-associated SCC. In this category, patients are younger at diagnosis, with increasing numbers under the age of 40 [3].

^{18}F-FDG PET/CT has demonstrated good sensitivity and specificity of around 80–100% in staging and following-up HNSCC [4-7], with no difference between HPV positive and negative. Angiogenesis plays a crucial role in tumor growth as well as in treatment resistance [3, 8] and represents an important target for the treatment of solid tumors with different expression of integrins on tumoral vessels in comparison with normal vessels [8-12]. Novel angiogenesis-targeting therapies have been developed with good response alone or in combination with conventional chemo-radiotherapies [13, 14]. Morphologic imaging like MRI can only indirectly show angiogenesis with injection of gadolinated contrast, but it is limited by procedure time, lack of sensitivity and absence of validated quantification. ^{68}Ga-NODAGA-RGD can be produced locally in centers with access to a ^{68}Ga generator [15] and radiolabeling can be easily done in kit-based or automated modules. It targets the $\alpha_v\beta_3$ integrins [8-10], and showed promising results in animal trials and demonstrated safe dosimetry profile [16-18]. Patients with different tumor types have also been reported using ^{68}Ga-NODAGA-RGD [16, 19, 20], but no specific study has been performed in a HNSCC population.

We aimed at evaluating the potential of ^{68}Ga-NODAGA-RGD PET/CT for imaging angiogenesis in HNSCC in comparison to the standard ^{18}F-FDG PET/CT regarding tumoral uptake and distribution, as well as histological differentiation.

Materials And Methods

Study population

Ten consecutive patients were prospectively enrolled with untreated HNSCC of the oral cavity, hypopharynx or rhinopharynx proven by histology. They were referred by the Department of Head and Neck Surgery to the Department of Nuclear Medicine and Molecular Imaging for a ^{18}F-FDG PET/CT. Written informed consent was obtained from study participants. Ethics committee approval was obtained for the protocol (Ethics Commission Vaud, protocol CER-VD #120/12) and from the Swiss national regulatory authorities. The inclusion criteria were age ≤ 85 years, Karnofsky index ≥ 80%, biopsy-proven HNSCC and signed consent form; exclusion criteria were pregnancy, breastfeeding and age < 18 years. The biopsy was performed at least 2 weeks before PET/CT imaging.

Image acquisitions

Both ^{18}F-FDG and ^{68}Ga-NODAGA-RGD PET/CT were performed at our hospital. Pregnancy test was done before the scan in women of childbearing age before each PET/CT. Patients were asked to fast > 6 hours before tracer injection and blood glucose was < 8.3 mmol/L before tracer injection. Vertex to mid-thigh acquisition (8 bed positions, 2 min per bed position, with dedicated 2 bed position acquisition of 3 minutes per bed position on ear, nose and throat (ENT) region [vertex to pulmonary apex]) was performed (Discovery 690 TOF, GE Healthcare, Waukesha, WI, USA). ^{68}Ga-NODAGA-RGD PET/CT images were acquired 70 min after intravenous administration of 200 MBq ^{68}Ga-NODAGA-RGD in an antecubital vein followed by 10 mL of 0.9% NaCl solution and ^{18}F-FDG images were acquired 70 minutes after intravenous injection of 3.5 MBq/kg ^{18}F-FDG in an antecubital vein followed by 10 mL of 0.9% NaCl solution. PET data were reconstructed using OSEM (3 iterations, 16 subsets). Head to mid-thigh unenhanced CT was acquired for attenuation correction (120kV, 60mA, 0.8s/rotation, pitch 0.9, CTDI 4.54 mGy). The mean delay between both PET/CT scans was ≤ 7 days.

Image analysis

Images were post-processed on an Advantage Workstation 4.6 (GE Healthcare, Waukesha, Wisconsin, USA) using multiplanar reformatted images of PET alone, CT alone and fused PET/CT with linked cursors. Image analysis was performed by two nuclear physicians with respectively 3 and 15-year experience in PET/CT. First, tracers' distribution was assessed by activity seen in normal anatomical structures and by measuring the maximum and mean SUV (SUV_{max} and SUV_{mean}) in the brain, parotid glands, thyroid, mediastinum, myocardium, lung, liver, spleen, colon, small intestine, kidneys, bladder, psoas muscle and bone marrow (i.e. first lumbar vertebra) from a 42% SUV_{max} thresholded volume of interest (VOI) embedding each structure. Tracers' uptake was then observed in the primary tumors, lymph nodes and distant metastases, as well as in any non-tumoral pathological structure. When available, magnetic resonance images were compared to PET images for precise localization of intra-tumoral uptake. Second, SUV_{max} and SUV_{mean} of the primary tumors, lymph nodes and metastases were semi-automatically extracted from a 3-D volume of interest (VOI) delineated around the lesion using a threshold-based with 42% SUV_{max}, as illustrated in Figure 1. Background uptake was measured in the posterior cervical muscles with a VOI of 1.5 cm^3 to compute the lesion-to-background ratio. Tracer avid tumor volume (TATV) is the volume within a boundary determined with a SUV_{max} 42%-threshold for ^{68}Ga-NODAGA-RGD. For ^{18}F-FDG PET, this same SUV_{max} 42%-threshold corresponds to usual metabolic tumor volume (MTV). The size of the lymph node was measured in its short axis.

Histopathological analysis

All histopathological biopsies were performed in the Department of Head and Neck Surgery and analyses in the Institute of Pathology by a pathologist specialized in head and neck cancers. The analysis of samples included standard histopathology analysis with evaluation of the tumor grade, as well as an immunostaining analysis of p16 and in situ hybridization to detect high risk HPV.

Statistical analysis

Continuous variables are presented as mean ± standard deviation (SD). SUV values were compared with the Wilcoxon signed-rank test for differences between ^{68}Ga-NODAGA-RGD and ^{18}F-FDG scans, as well as for the effect of tumor grade, HPV and p16 status. The relation between ^{68}Ga-NODAGA-RGD and ^{18}F-FDG values was assessed using the Spearman correlation coefficient, which was also used to assess the relation between tracers' uptake and age or lymph node size. Statistics were performed with the Stata 15.1 software (StataCorp, College Station, TX, USA). A p-value <0.05 was considered as statistically significant.

Results

Study population

We included 10 patients (6 males and 4 females), all Caucasian with a mean age of 58.4 ± 8.3 years (range: 44–73 years). All patients had a proven head and neck squamous cell carcinoma, with one patient (#5) having two synchronous tumors (1 HNSCC and 1 dedifferentiated carcinoma) (Table 1). Histologic grading showed only 2 patients with poorly differentiated tumor, 4 were well differentiated, and 5 had a moderate differentiation. Finally, one patient (#5) had distant metastasis (2 lung lesions).

PET/CT imaging

PET/CT images were acquired 71 ± 14 minutes (range: 56–90 minutes) after administration of 216 ± 79 MBq (range: 208–250 MBq) ^{68}Ga-NODAGA-RGD. For ^{18}F-FDG, images were acquired 70 ± 11.5 minutes (range: 63–93 minutes) after injection of 3.5 MBq/kg (range: 185-291 MBq). The mean time elapsed since ^{18}F-FDG and ^{68}Ga-NODAGA-RGD PET/CT scans was 2.5 ±1.8 days (range: 1–7 days). Both radiopharmaceuticals were well-tolerated, and no radiopharmaceutical-related adverse effect was observed. The mean time elapsed since biopsy and PET/CT imaging was 17.5 ± 5.3 days (range: 14–24 days)

^{68}Ga-NODAGA-RGD distribution

^{68}Ga-NODAGA-RGD in comparison to ^{18}F-FDG PET/CT images demonstrated different whole-body distributions in all the ten patients. Figure 2 displays body tracers' distribution of four selected patients. Compared to ^{18}F-FDG images, ^{68}Ga-NODAGA-RGD images demonstrated significantly higher uptake in the spleen and in the kidneys, while the uptake was lower in the brain, the parotid glands, the mediastinum, the myocardium, the lung, the liver, the psoas muscle and the bone (all p<0.037, Figure 3). Similar uptake were measured in the thyroid gland, the gut and the bladder (all p>0.1).

Non-tumoral positive uptake regions were seen in several patients for both tracers, notably due to inflammatory diseases. The majority of them were seen in patients #1, #4, #5 and #6 and were analyzed as glenohumeral joint inflammation proven by clinical data. In patients #1, #2 and #6, stomatitis was proven by mouth and throat examination.

Analysis in the primary tumors

All primary tumours were visually detectable with both tracers (Table 2). Distribution of the tracers within the tumors was different as shown on the axial PET/CT fusion (Figure 1). Compared to magnetic resonance images for tumour delineation, we noticed that ^{18}F-FDG uptake was mostly homogenous inside the tumors. ^{68}Ga-NODAGA-RGD PET showed heterogenous uptake within the tumors. In patients #8 (Figure 4) for instance, moderate uptakes were seen mostly in the periphery of the tumor. Necrotic areas did not display significant uptake for both tracers (Figure 5).

Tumor uptake was significantly higher with ^{18}F-FDG than with ^{68}Ga-NODAGA-RGD (SUV_{max} 14.0 ± 6.1 g/mL versus 3.9 ± 1.1 g/mL, p=0.0017; SUV_{mean} (8.2 ± 3.1 g/mL versus 2.0 ± 0.8 g/mL, p=0.0017) as was the tumor-to-background ratio (Table 2). One patient showed very low ^{68}Ga-NODAGA-RGD activity (patient #9). A linear positive correlation between the ^{18}F-FDG and the ^{68}Ga-NODAGA-RGD SUV_{mean} was found (Spearman's rho=0.89, p=0.0068), but not for SUV_{max} values (Spearman's rho=0.39, p=0.38). There was no statistically significant relation between age and tracers' uptake (p= 0.5). As seen in Table 2, "tracer avid tumor volume" was larger with ^{68}Ga-NODAGA-RGD PET/CT with a volume around 30% higher for ^{68}Ga-NODAGA-RGD (Figure 6), but this difference did not reach statistical significance (p=0.085) in comparison to ^{18}F-FDG PET/CT. There was no significant correlation between the uptake volumes of the two tracers (Spearman's rho= 0.038, p<0.05).

Analysis in the lymph nodes and metastases

All lymph nodes and distant metastases were seen with both tracers. In some cases, such as in patients #9 and #10, ^{68}Ga-NODAGA-RGD uptake was however very low, with a target-to-background ratio <2. The size of the lymph node was measured in short axis (8.5 ± 2.7 mm, range: 4–15 mm), and there was no significant correlation between lymph node size and uptake (p> 0.05). Tracer avid tumor volume was always higher with the ^{68}Ga-NODAGA-RGD PET in the lymph nodes, as seen with in the primary tumors.

Metastatic spread of the disease was seen only in patient #5, with bilateral lung metastases. Lower SUV_{max} was reported with the ^{68}Ga-NODAGA-RGD PET (7.7 g/mL versus 11.9 g/mL), and higher tracer avid tumor volume (2.8 mL versus 0.8 mL). No statistical analysis of metastatic disease was performed because of the paucity of lesions.

Effect of tumor grade, p16 and HPV status

Both radiotracers' uptakes did not correlate with tumor grade (p≥0.17). P16 and HPV immunostaining showed a good association between the p16 and HPV tests (p<0.05). Five histopathological analyses were HPV and p16 positive and six were negative. Mean SUV_{max} values of p16 and HPV positive cases were 16.4 ± 6.9 g/mL with ^{18}F-FDG and 3.8 ± 1.0 g/mL with ^{68}Ga-NODAGA-RGD. Mean SUV_{max} values of p16 and HPV negative cases were respectively of 9.8 ± 1.7 g/mL with ^{18}F-FDG and 4.1 ± 1.2 g/mL with ^{68}Ga-NODAGA-RGD. No significant difference in both tracers' uptake was found regarding HPV or p16 protein expression (p=0.22) (Table 4).

Discussion

Our pilot study is the first study on humans to systematically compare ^{18}F-FDG and ^{68}Ga-NODAGA-RGD uptake in a HNSCC patient population. It shows that: (1) every primary HNSCC tumour and lymph nodes were visually detectable with both tracers, but with different uptake patterns; (2) ^{68}Ga-NODAGA-RGD uptake was heterogeneous with a low target-to-background ratio while ^{18}F-FDG uptake is mostly homogeneous with higher target-to-background ratio; and (3) ^{68}Ga-NODAGA-RGD uptake was not related to tumor grade, p16 or HPV status.

^{18}F-FDG PET-CT has a high clinical value in the initial workup and follow-up of patients with HNSCC tumors [4-7]. It however only allows evaluation of tumor cells metabolism but not neoangiogenesis. To this purpose we conducted a one-to-one comparison of tracers to assess the clinical potential of ^{68}Ga-NODAGA-RGD. All HNSCC primary tumors, lymph nodes and metastases detected on ^{18}F-FDG PET/CT images were also seen with the angiogenesis radiotracer. Only few studies have been conducted in humans; while Haubner et al. [20] demonstrated that ^{68}Ga-NODAGA-RGD uptake was not sufficient to be used in patients with hepatocellular carcinoma, other authors reported sufficient uptake for diagnostic purpose in human xenografts of esophageal carcinoma, melanoma and glioblastoma [18, 21]. As both ^{68}Ga-NODAGA-RGD and ^{18}F-Galacto-RGD demonstrated similar preclinical results [22], our results are in line with the previous work by Beer et al. [8], who concluded that thanks to its significant uptake, ^{18}F-Galacto-RGD might be used for the assessment of angiogenesis and for planning and response evaluation of $\alpha_v\beta_3$ targeted therapies in HNSCC.

However, it is worth to mention that tracer uptake patterns were very different between ^{18}F-FDG and ^{68}Ga-NODAGA-RGD. Indeed, TATV were larger with ^{68}Ga-NODAGA-RGD, with heterogeneous uptake within the primary tumor and lymph nodes, and relative low target-to-background ratio compared with ^{18}F-FDG. While this seems to preclude the use of ^{68}Ga-NODAGA-RGD as a single tracer for tumor staging, we assume that it brings complementary information about the tumor itself. Part of volume difference can be due to difference in positron energy between the fluorine-18 and gallium-68. Also, the threshold used for TATV delineation is subject to discussion. We used a 42% SUV_{max} fixed threshold similarly to MTV delineation, which may have resulted in larger TATV due to lower SUV_{max} values with ^{68}Ga-NODAGA-RGD. Threshold adaptation for ^{68}Ga-NODAGA-RGD could be performed defined based on tumor margins if defined on whole tumor histopathological specimen, which was out of the scope of our study, as not all tumors and lymph nodes were resected in toto. Nevertheless, we believe that difference in uptake patterns and volume are mainly attributable to difference in the tracer targeting. Although we did not perform the immunohistochemistry staining of human HNSCC tissue microarray to properly correlate uptake with angiogenesis [23], it is known that ^{68}Ga-NODAGA-RGD

improves imaging of $\alpha_v\beta_3$ expression [24]. Beer et al. [8] demonstrated that the uptake of ^{18}F-Galacto-RGD mostly represented $\alpha_v\beta_3$ expression in the neovasculature, but not in the HNSCC tumor cells themselves. This was also confirmed with other RGD-based tracers on HNSCC tumor xenografts [25]. ^{68}Ga-NODAGA-RGD uptake beyond ^{18}F-FDG avid areas could thus reflect the presence of the formation of neovessels. Isal et al. [21] demonstrated that tumor areas with high ^{68}Ga-NODAGA-RGD uptake also exhibited the highest rates of cell proliferation and integrins expressions irrespective of cell density in engrafted glioblastomas. This seems to be different in HNSCC, as we did not find any significant association between tracers' uptake and HNSCC grade. Despite different uptake patterns, we found a significant correlation between ^{18}F-FDG and ^{68}Ga-NODAGA-RGD SUV_{mean} values, which overall might indicate the coexistence of interrelated pathophysiological phenomenon within the tumor, i.e. cell proliferation and neoangiogenesis. Finally, no significant difference in ^{68}Ga-NODAGA-RGD activity was found regarding HPV or p16 protein expression ($p \geq 0.22$). Although HPV and p16 have demonstrated significant prognostic value in HNSCC tumors [1, 26], this may not preclude the use of ^{68}Ga-NODAGA-RGD as a prognostic biomarker. Indeed, taking into account that tumor neovessels are of paramount importance for tumor oxygenation, the prognostic value of ^{68}Ga-NODAGA-RGD could be assessed in HNSCC patients undergoing chemoradiotherapy. Recent preclinical [27] and clinical pilot studies [28] hence reported that ^{111}In-RGD2 and ^{18}F-RGD-K5, two tracers targeting integrin $\alpha_v\beta_3$, having the potential to monitor response to therapy and to identify patients with incomplete responses to concurrent chemoradiotherapy. This point has to be explored in a larger prospective study.

We acknowledge several limitations inherent to a pilot study. First, we evaluated a small sample of HNSCC patients, which limits discriminating power, especially regarding correlation with histology. Second, immunostaining was not performed to confirm regional $\alpha_v\beta_3$ expression, but rather characterize whole tumor distribution. Third, as already mentioned, we used a fixed threshold for TATV definition in a first approximation, which might have overestimated tumor volume; threshold optimization based on spatial comparison with $\alpha_v\beta_3$ immunostaining on whole-tumor histological slices would need to be performed for more precision. Finally, larger, longitudinal studies would need to be performed to determine the prognostic value of ^{68}Ga-NODAGA-RGD.

Conclusion

Our study revealed that HNSCC primary tumors, lymph nodes and pulmonary metastasis can be visualized with both ^{18}F-FDG and ^{68}Ga-NODAGA-RGD PET/CT. While SUV_{mean} values were correlated among both tracers, intensity were largely different and were not influenced by HPV or p16 status. This indicates potential complementary use of both tracers. Further studies are now needed to elucidate the respective role of ^{68}Ga-NODAGA-RGD in the workup of patients with HNSCC.

Declarations

Ethical Approval and Consent to participate

All procedures performed in this study involving human participants were in accordance with the ethical standards of the institutional research committee and with the 1964 Helsinki declaration and its later amendments or comparable ethical standards. The name of the ethical committee is *"Ethics Committee Vaud"*, the reference number is CER-VD #120/12.

Written informed consent was obtained from all patients.

Consent for publication

Not applicable.

Availability of data and materials

The datasets used and/or analyzed during the current study are available from the corresponding author on reasonable request.

Competing interests

The authors declare that they have no competing interests.

Funding

The authors are indebted to the Leenaards Foundation (J. Prior) and the Swiss Cardiology Foundation (Bern, Switzerland) for their financial support in conducting this study.

Authors' contributions

SD drafted the manuscript, recruited some of the patients and performed part of the statistical analysis. VD participated in the design of the study and performed the statistical analysis and helped to draft the manuscript. FG recruited some of the patients. PM and NS helped in the PET/CT analysis. JD allowed production of the radiotracer and carried out the quality control of the radiotracer.

JOP conceived of the study, participated in its design and coordination and helped to draft the manuscript. All authors read and approved the final version of manuscript.

Acknowledgments

They would like to thank Dr. Franz Buchegger, MD (retired from the Department of Nuclear Medicine and Molecular Imaging, Lausanne University Hospital, Lausanne, Switzerland) and Dr. Marek Kosinski, PhD (retired from Applied Radiophysics Institute, Lausanne University Hospital, Lausanne, Switzerland), as well as Ms. Christine Geldhof from our Nuclear Medicine and Molecular Imaging Department for their help in this study.

Authors' information

Not applicable.

References

1. Mirghani H, Bellera C, Delaye J, Dolivet G, Fakhry N, Bozec A, et al. Prevalence and characteristics of HPV-driven oropharyngeal cancer in France. Cancer Epidemiol. 2019;61:89-94. doi:10.1016/j.canep.2019.05.007.
2. Broglie MA, Stoeckli SJ, Sauter R, Pasche P, Reinhard A, de Leval L, et al. Impact of human papillomavirus on outcome in patients with oropharyngeal cancer treated with primary surgery. Head Neck. 2017;39:2004-15. doi:10.1002/hed.24865.
3. Chaturvedi AK, Engels EA, Pfeiffer RM, Hernandez BY, Xiao W, Kim E, et al. Human papillomavirus and rising oropharyngeal cancer incidence in the United States. J Clin Oncol. 2011;29:4294-301. doi:10.1200/JCO.2011.36.4596.
4. Escott EJ. Role of positron emission tomography/computed tomography (PET/CT) in head and neck cancer. Radiol Clin North Am. 2013;51:881-93. doi:10.1016/j.rcl.2013.05.002.
5. Helsen N, Van den Wyngaert T, Carp L, De Bree R, VanderVeken OM, De Geeter F, et al. Quantification of 18F-fluorodeoxyglucose uptake to detect residual nodal disease in locally advanced head and neck squamous cell carcinoma after chemoradiotherapy: results from the ECLYPS study. Eur J Nucl Med Mol Imaging. 2020. doi:10.1007/s00259-020-04710-4.
6. Rohde M, Dyrvig AK, Johansen J, Sorensen JA, Gerke O, Nielsen AL, et al. 18F-fluoro-deoxy-glucose-positron emission tomography/computed tomography in diagnosis of head and neck squamous cell carcinoma: a systematic review and meta-analysis. Eur J Cancer. 2014;50:2271-9. doi:10.1016/j.ejca.2014.05.015.
7. Van den Wyngaert T, Helsen N, Carp L, Hakim S, Martens MJ, Hutsebaut I, et al. Fluorodeoxyglucose-Positron Emission Tomography/Computed Tomography After Concurrent Chemoradiotherapy in Locally Advanced Head-and-Neck Squamous Cell Cancer: The ECLYPS Study. J Clin Oncol. 2017;35:3458-64. doi:10.1200/JCO.2017.73.5845.
8. Beer AJ, Grosu AL, Carlsen J, Kolk A, Sarbia M, Stangier I, et al. [18F]galacto-RGD positron emission tomography for imaging of alphavbeta3 expression on the neovasculature in patients with squamous cell carcinoma of the head and neck. Clin Cancer Res. 2007;13:6610-6. doi:10.1158/1078-0432.CCR-07-0528.
9. Beer AJ, Haubner R, Goebel M, Luderschmidt S, Spilker ME, Wester HJ, et al. Biodistribution and pharmacokinetics of the alphavbeta3-selective tracer 18F-galacto-RGD in cancer patients. J Nucl Med. 2005;46:1333-41.
10. Beer AJ, Haubner R, Sarbia M, Goebel M, Luderschmidt S, Grosu AL, et al. Positron emission tomography using [18F]Galacto-RGD identifies the level of integrin alpha(v)beta3 expression in man. Clin Cancer Res. 2006;12:3942-9. doi:10.1158/1078-0432.CCR-06-0266.
11. Schnell O, Krebs B, Carlsen J, Miederer I, Goetz C, Goldbrunner RH, et al. Imaging of integrin alpha(v)beta(3) expression in patients with malignant glioma by [18F] Galacto-RGD positron emission tomography. Neuro Oncol. 2009;11:861-70. doi:10.1215/15228517-2009-024.
12. Beer AJ, Niemeyer M, Carlsen J, Sarbia M, Nahrig J, Watzlowik P, et al. Patterns of alphavbeta3 expression in primary and metastatic human breast cancer as shown by 18F-Galacto-RGD PET. J Nucl Med. 2008;49:255-9. doi:10.2967/jnumed.107.045526.
13. Al-Abd AM, Alamoudi AJ, Abdel-Naim AB, Neamatallah TA, Ashour OM. Anti-angiogenic agents for the treatment of solid tumors: Potential pathways, therapy and current strategies - A review. J Adv Res. 2017;8:591-605. doi:10.1016/j.jare.2017.06.006.
14. Kong DH, Kim MR, Jang JH, Na HJ, Lee S. A Review of Anti-Angiogenic Targets for Monoclonal Antibody Cancer Therapy. Int J Mol Sci. 2017;18. doi:10.3390/ijms18081786.
15. Zhernosekov KP, Filosofov DV, Baum RP, Aschoff P, Bihl H, Razbash AA, et al. Processing of generator-produced 68Ga for medical application. J Nucl Med. 2007;48:1741-8. doi:10.2967/jnumed.107.040378.
16. Gnesin S, Mitsakis P, Cicone F, Deshayes E, Dunet V, Gallino AF, et al. First in-human radiation dosimetry of (68)Ga-NODAGA-RGDyK. EJNMMI Res. 2017;7:43. doi:10.1186/s13550-017-0288-x.

17. Gaertner FC, Kessler H, Wester HJ, Schwaiger M, Beer AJ. Radiolabelled RGD peptides for imaging and therapy. Eur J Nucl Med Mol Imaging. 2012;39 Suppl 1:S126-38. doi:10.1007/s00259-011-2028-1.
18. Zhai C, Franssen GM, Petrik M, Laverman P, Summer D, Rangger C, et al. Comparison of Ga-68-Labeled Fusarinine C-Based Multivalent RGD Conjugates and [(68)Ga]NODAGA-RGD-In Vivo Imaging Studies in Human Xenograft Tumors. Mol Imaging Biol. 2016;18:758-67. doi:10.1007/s11307-016-0931-3.
19. Van Der Gucht A, Pomoni A, Jreige M, Allemann P, Prior JO. 68Ga-NODAGA-RGDyK PET/CT Imaging in Esophageal Cancer: First-in-Human Imaging. Clin Nucl Med. 2016;41:e491-e2. doi:10.1097/RLU.0000000000001365.
20. Haubner R, Finkenstedt A, Stegmayr A, Rangger C, Decristoforo C, Zoller H, et al. [(68)Ga]NODAGA-RGD - Metabolic stability, biodistribution, and dosimetry data from patients with hepatocellular carcinoma and liver cirrhosis. Eur J Nucl Med Mol Imaging. 2016;43:2005-13. doi:10.1007/s00259-016-3396-3.
21. Isal S, Pierson J, Imbert L, Clement A, Collet C, Pinel S, et al. PET imaging of (68)Ga-NODAGA-RGD, as compared with (18)F-fluorodeoxyglucose, in experimental rodent models of engrafted glioblastoma. EJNMMI Res. 2018;8:51. doi:10.1186/s13550-018-0405-5.
22. Pohle K, Notni J, Bussemer J, Kessler H, Schwaiger M, Beer AJ. 68Ga-NODAGA-RGD is a suitable substitute for (18)F-Galacto-RGD and can be produced with high specific activity in a cGMP/GRP compliant automated process. Nucl Med Biol. 2012;39:777-84. doi:10.1016/j.nucmedbio.2012.02.006.
23. Liu JF, Deng WW, Chen L, Li YC, Wu L, Ma SR, et al. Inhibition of JAK2/STAT3 reduces tumor-induced angiogenesis and myeloid-derived suppressor cells in head and neck cancer. Mol Carcinog. 2018;57:429-39. doi:10.1002/mc.22767.
24. Knetsch PA, Petrik M, Griessinger CM, Rangger C, Fani M, Kesenheimer C, et al. [68Ga]NODAGA-RGD for imaging alphavbeta3 integrin expression. Eur J Nucl Med Mol Imaging. 2011;38:1303-12. doi:10.1007/s00259-011-1778-0.
25. Terry SY, Abiraj K, Frielink C, van Dijk LK, Bussink J, Oyen WJ, et al. Imaging integrin alphavbeta3 on blood vessels with 111In-RGD2 in head and neck tumor xenografts. J Nucl Med. 2014;55:281-6. doi:10.2967/jnumed.113.129668.
26. Okami K. Clinical features and treatment strategy for HPV-related oropharyngeal cancer. Int J Clin Oncol. 2016;21:827-35. doi:10.1007/s10147-016-1009-6.
27. Terry SY, Abiraj K, Lok J, Gerrits D, Franssen GM, Oyen WJ, et al. Can 111In-RGD2 monitor response to therapy in head and neck tumor xenografts? J Nucl Med. 2014;55:1849-55. doi:10.2967/jnumed.114.144394.
28. Chen SH, Wang HM, Lin CY, Chang JT, Hsieh CH, Liao CT, et al. RGD-K5 PET/CT in patients with advanced head and neck cancer treated with concurrent chemoradiotherapy: Results from a pilot study. Eur J Nucl Med Mol Imaging. 2016;43:1621-9. doi:10.1007/s00259-016-3345-1.

Tables

	Gender	Age	TNM	Tumor localization	Biopsy result	Histologic grading	p16	HPV
1	F	63	pT2 pN1 cM0	Left tonsil	SCC	Poorly differentiated	+	+
2	M	59	pT2 pN1 cM0	Left tonsil	SCC	Well differentiated	–	–
3	M	53	pT2 pN2b cM0	Left paramandibular	SCC	Moderate differentiated	+	+
4	M	50	pT3 pN0 cM0	Left arytenoid	SCC	Well differentiated	+	+
5	F	73	pT1b pN2b cM1	Glottic	SCC	Well differentiated	–	–
	F	73	pT3 pN2b pM1	Posterior oral cavity	SCC	Well differentiated	–	–
6	F	65	pT4a pN2c cM0	Right tongue base	SCC	Moderate differentiated	+	+
7	M	49	cT2 cN3b cM0	Left tonsil	SCC	Moderate differentiated	–	–
8	F	69	pT4a pN2c cM0	Base of the tongue	SCC	Moderate differentiated	–	–
9	M	59	pT3 pN3 cM0	Left tonsil	SCC	Moderate differentiated	–	–
10	M	44	pT2 pN2 cM0	Right rhinopharynx	Dedifferentiated carcinoma	Poorly differentiated	+	+

Table 1
Study population

Patient	SUVmax [g/mL]		SUVmean [g/mL]		SUV42%/SUVbackground [1]		Tracer avid tumor volume [cm^3]	
	FDG	RGD	FDG	RGD	FDG	RGD	FDG	RGD
1	11.6	3.5	9.1	2.4	9.3	3.3	3.7	21
2	14.3	2.5	12.5	2.9	15.3	5	2.3	12.9
3	20.6	5.2	9	2.1	16.6	3.8	10.5	34.7
4	10.6	3.2	6.7	1.9	10.8	2.7	2.4	8.1
5	7.6	3.1	5.5	0.4	10.8	2.8	1.2	3.5
	9.7	4.8	8.7	2.7	8.7	4.4	4.2	12.3
6	16.6	4.4	10.4	2.8	9.1	4.8	8.5	17
7	8.6	4.8	5	2.7	9.5	5.3	5	6.4
8	8.5	4.5	5.3	2.3	7.7	4.8	28.6	38
9	8.7	2.1	4.9	0.9	9.6	2	6	8.1
10	28.3	2.3	14	1.2	31.4	2.5	10	16
Mean	14	3.9	8.2	2.0	12.7	3.8	9.6	14
SD	6.1	1.1	3.1	0.8	4.6	1.0	11.2	9.4
p		0.0017		0.0017		0.0017		0.085

Table 2
SUV and TATV results of primary tumors

Patient	Localization	Dimension [1] [mm]	SUVmax [g/mL]		SUVmean [g/mL]		SUV42%/SUVbackground [1]		Tr tu [c
		FDG	RGD	FDG	RGD	FDG	RGD	FDG	
1	Left IIb	10	3	3.2	1.9	2	3.3	4.5	3.
2	Left IIa	9	4.7	1.3	2.6	0.8	4.3	2.2	3.
3	Left IIa–IIb	4	15	3.1	8.4	1.8	16.6	3.9	8.
4	None	–	–	–	–		–	–	–
5	Right IIa	10	11.2	2.8	6.7	1.8	14	3.5	1
	Right IIa	9	13	4.8	9	2.9	16.2	6	3.
	Right IIa	6	3.9	3.5	2.3	2.1	4.9	4.4	2.
6	Left IIa	8	7.7	3.5	4.5	2	8.5	4.4	1.
	Right III	15	6	2.2	3.6	1.2	6.7	2.8	1.
	Left III	9	5.2	2.5	3	1.4	5.8	3.1	1.
	Right IV	7	6	1.9	3.7	1.1	6.7	2.4	1.
	Left IV	7	7.8	1.9	4.6	1.2	8.7	2.4	1.
	Right V	7.5	7.4	1.7	4.8	1	8.2	2.1	1
7	Right IIa	9	4	1.9	2.2	1.1	4.4	2.4	3
	Left IIb	5	2.3	2.4	1.3	1.3	2.5	3	3.
8	Right IIa	14	4	1.2	2.5	0.9	4.4	1.5	4
	Right IIb	13	7	2.4	4.1	1.4	7.8	3	3.
9	Left I	17	4	1.3	2.1	1	4.4	1.6	5.
	Left IIa	17	4.5	1.4	2.4	1	5	1.7	6
	Left IIb	12	4	1.4	2.1	0.9	4.4	1.7	4.
	Left III	13	5	2.2	3	1.2	5.5	2.7	4
10	Left retropharyngeal	7	7	1.4	4.1	1	7.8	1.7	5.
	Right retropharyngeal	5	4	1	2	0.8	4.4	1.2	3
	Right IIa	7	7	1.5	4	1.3	7.8	1.9	5
Mean		8.5	7	2.5	3.5	1.3	6.8	2.8	3.
SD		2.7	4.1	1.2	2.6	0.7	5	1.5	2.
P				0.0017		0.0017		0.0017	
5	Pulmonary Right upper lobe	16	12	2.3	7.7	1.4	15	2.9	0.
	Pulmonary left upper lobe	10	11.8	1.2	7.7	0.7	14.8	1.5	0.
Mean			11.9	1.7	7.7	0.8	14.9	2.2	0.

[1]Lymph node measure: small axis.

Table 3
SUV and TATV results of lymph nodes and distant metastases

	HPV AND p16 POSITIVE		HPV AND p16 NEGATIVE	
	FDG	RGD	FDG	RGD

	HPV AND p16 POSITIVE		HPV AND p16 NEGATIVE	
	14.3	4.3	10.6	5.4
	15.7	4.2	9.7	3.1
	10.6	3.2	13	4.8
	13	4.8	8.6	4.8
			8.5	4.5
	28.3	2.3	8.7	2.1
Mean	16.4	3.8	9.8	4.1
SD	6.9	1.0	1.7	1.2
p	0.22		0.22	

Table 4
SUV_{max} of HPV – p16 positive and negative cases

Figures

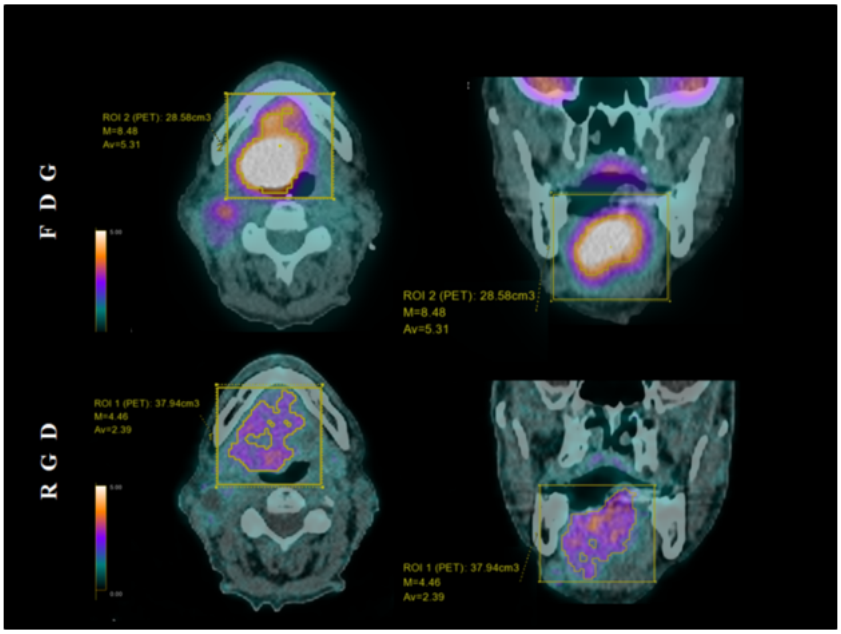

Figure 1

Example of axial and coronal 18F-FDG and 68Ga-NODAGA-RGD PET/CT 3-D volume of interest semi-automatically delineated on a SUVmax 42%-threshold for patient #8 using a parallelepipedal bounding box.

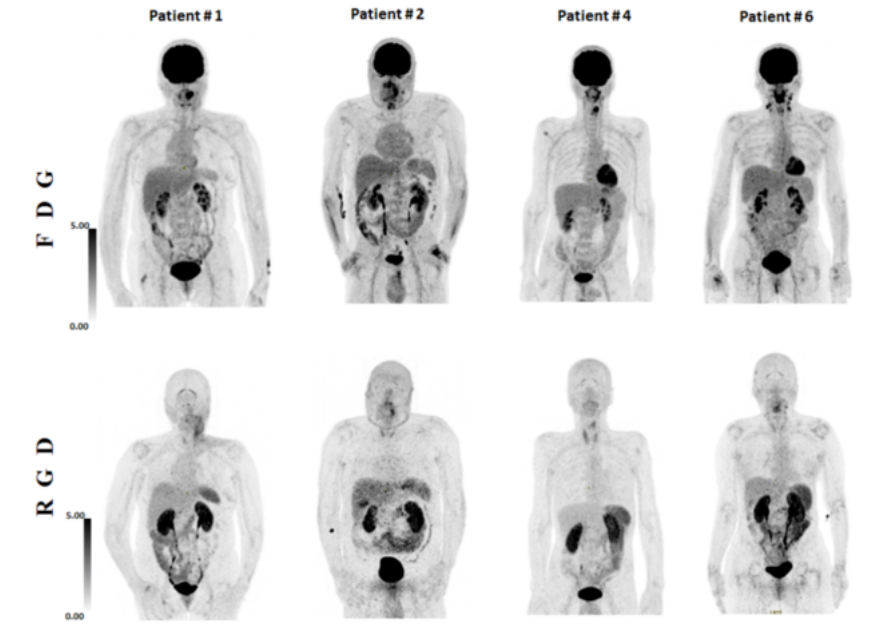

Figure 2

Maximum intensity projection (MIP) of 18F-FDG and 68Ga-NODAGA-RGD PET/CT in four patients. HNSCC primary tumor had a significant uptake in all patients. Lymph nodes also demonstrated a significant uptake as seen in patients 1 and 6. A focal uptake is detectable withy 68Ga-NODAGA-RGD PET/CT in the liver of patient#2, corresponding to the gallbladder. Inflammatory capsulitis of the glenohumeral joint was also observed in patients # 1 and # 6.

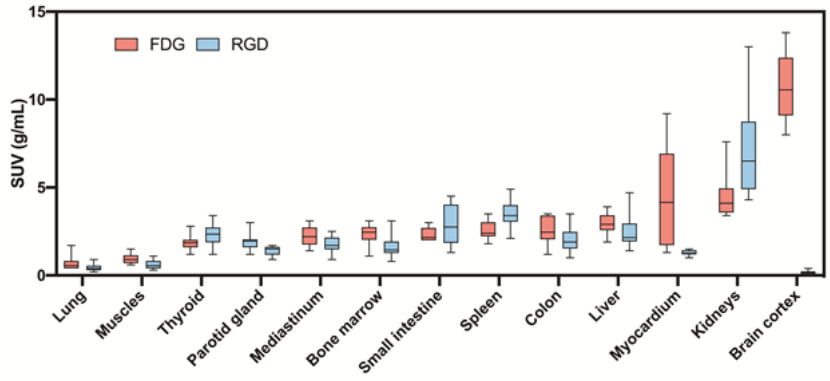

Figure 3

Box plot comparison of 18F-FDG and 68Ga-NODAGA-RGD SUVmax in organs. SUVmax was significantly different between both tracers in all organs (all $p<0.037$), except in the thyroid, the gut (small intestine and colon) and the bladder (not shown) (all $p>0.10$). The most significant difference was observed for the brain and the myocardium, which presented only minimal 68Ga-NODAGA-RGD uptake compared to 18F-FDG.

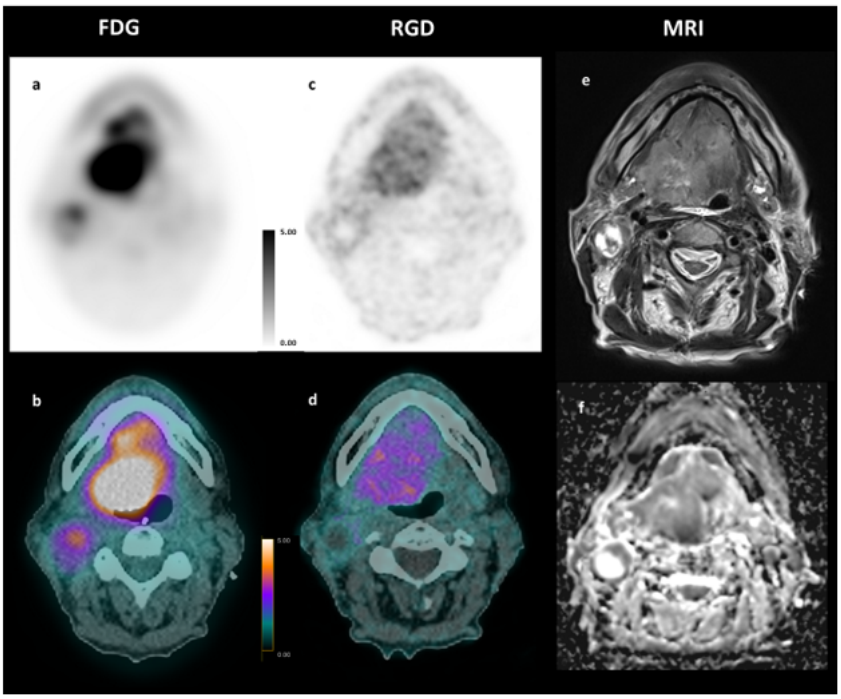

Figure 4

Comparative MRI, 18F-FDG and 68Ga-NODAGA-RGD PET/CT of patient # 8. Axial PET/CT fusion slices of a 69 years old man with a moderate differentiated base tong SCC. The images show different tumor-to-background ratios in-between the two radiotracers 18F-FDG PET/CT (a-b) vs. 68Ga-NODAGA-RGD PET/CT (c-d), and also a slightly different distribution of activity within the tumor bed when compared with the MR images (e) T2w and (f) ADC map of diffusion.

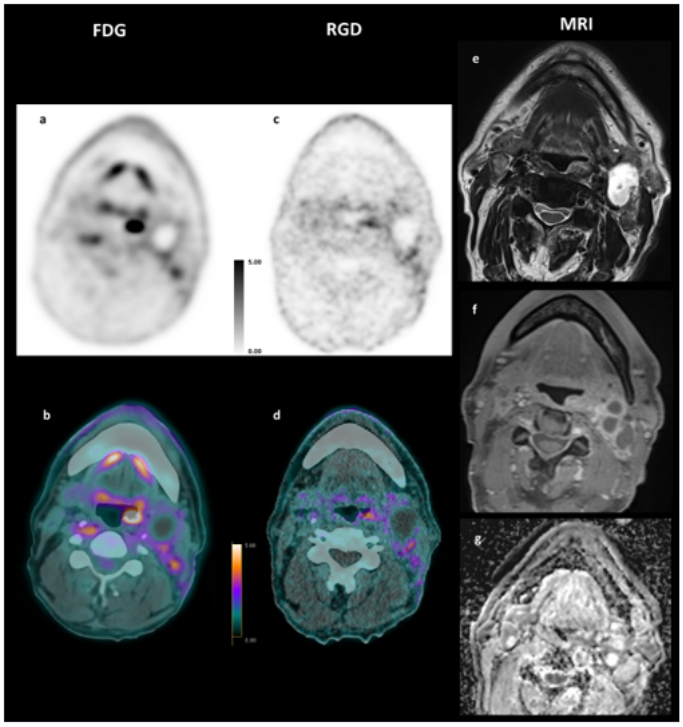

Figure 5

Comparative 18F-FDG (a-b), 68Ga-NODAGA-RGD PET/CT (c-d) and MRI (e: T2w axial, f: T1w post Gadolinium, g: ADC map of diffusion), of patient # 9 (59-year man with moderate differentiated left tonsil squamous cell carcinoma). The 18F-FDG and 68Ga-NODAGA-RGD PET images showed different signal-to-noise ratios, and a slightly different distribution of activity within the tumor bed. The left cervical lymph node showed a photopenic center with absence of tracer uptake for both tracers corresponding to necrosis on MRI.

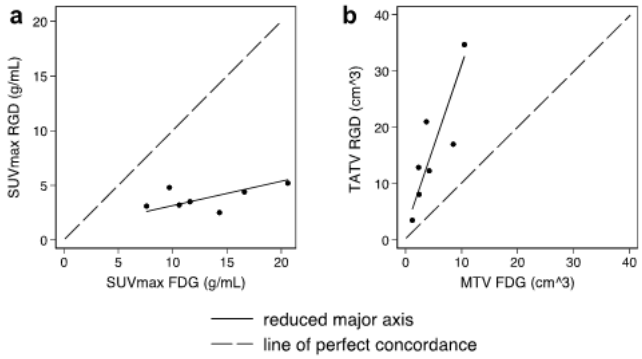

Figure 6

Correlation between (a) 18F-FDG and 68Ga-NODAGA-RGD SUVmax, which was systematically lower (slope of the reduced major axis 0.22 < 1.00) and (b) 68Ga-NODAGA-RGD tracer avid tumor volume (TATV), which was systematically higher than 18F-FDG metabolic tumor volume (MTV) (slope of the reduced major axis 2.91 > 1.00).